JOURNAL OF MATERIALS SCIENCE **36** (2001) 3437–3446

Effect of sintering temperature and holding time on the properties of 3Y-ZrO_2 microfiltration membranes

F. SHOJAI, T. A. MÄNTYLÄ
Tampere University of Technology, Institute of Materials Science, P. O. Box 589, FIN-33101 Tampere, Finland
E-mail: fshojai@hotmail.com

Sintering behavior of supported and unsupported microfiltration membranes prepared from 3 mol% yttria doped zirconia powder was investigated as a function of temperature and holding time in non-isothermal and isothermal densification. Shrinkage that started at 1000°C showed the highest rate between 1200°C and 1300°C although the rate decreased above 1300°C. The activation energy of sintering was calculated at 735 kJ/mol, assuming the grain boundary diffusion mechanism for mass transport. Mean pore size decreased in unsupported membranes and increased in supported ones as the sintering temperature increased up to 1200°C. Dimensional shrinkage of unsupported membrane slabs showed an increase in shrinkage first in the lateral dimension and then in the thickness as the sintering temperature increased. Pore growth and lower hardness in supported membranes, can be explained due to the restricted lateral shrinkage in the supported membranes. Removal of porosity was pronounced above 1100°C and the density increased linearly as a function of holding time. Microhardness of membranes sintered above 1100°C increased as a function of sintering temperature and was higher in unsupported membranes. Samples sintered above 975°C had a100% tetragonal phase structure. Permeability of supported membranes increased as a function of sintering temperature due to pore growth despite a decrease in porosity.

1. Introduction

Ceramic membranes offer many potential advantages over commercial organic membranes for separation processes due to high strength, the capability to be used at high temperatures and in harsh chemical environments [1]. Especially ceramic oxide membranes based on alumina, zirconia and titania have attracted attention in recent years [2, 3]. An oxide membrane, employed in separation processes with a pressure gradient, consists of a thin separation layer and a porous carrier, which serves as a support.

Zirconia membranes exhibit superior chemical resistance in harsh chemical environment especially in highly basic media [4]. Dense yttria-doped zirconia polycrystals (Y-TZP) with tetragonal structure exhibit high strength and toughness as compared to other ceramics [5]. It is interesting to know whether porous Y-TZP benefits from the same exceptional properties of the dense counterpart, such as high toughness due to phase transformation toughening mechanism. However, the instability of tetragonal phase in humid atmosphere at low temperatures (65–500°C), is the disadvantage of yttria-doped zirconia ceramics. This phenomenon has been discussed in dense ceramics extensively [6–9]. Zirconia microfiltration membranes with mean pore size of 0.1–0.2 μm which was produced in this work are currently used in fruit juice filtration, waste water treatment, dairy industry and have potential applications in mineral processing and many other industries [10].

Sintering of Y-ZrO_2 ceramics has been discussed regarding the microstructural development, changes in density, pore and grain growth and mechanism of sintering in many papers [11–21]. However, there are few studies on the preparation and characterization of Y-ZrO_2 membranes which concern mostly ultrafiltration applications [22–27] and a study on the sintering behavior and properties of 3Y-ZrO_2 microfiltration membrane prepared from well-characterized powder is lacking.

Expanding the application of zirconia membranes depends on the capability to tailor the properties to meet the demands of service conditions and it relies on the knowledge of processing of the green membrane as well as the evolution of properties during sintering. In this work, the influence of densification on the main properties of 3Y-ZrO_2 microfiltration membrane such as porosity, pore size distribution, hardness and permeability is studied.

2. Experimental procedure

2.1. Membrane material

Yttria doped zirconia 3Y-ZrO_2 powder HSY3, supplied by Zirconia Sales (UK), was used to produce membranes. Particle size and particle size distribution of powder were measured by laser diffraction method (Helos, Sympatec GmbH) in a diluted dispersion of powder after addition of dispersant, milling and sonication to insure the optimum disintegration of agglomerates. Specific surface area was measured by nitrogen adsorption using the BET method (DeSorb/FlowSorb II 2300A, Micromeritics). The chemical analysis of powder was measured by X-ray fluorescence XRF (PW 1400, Philips). Microstructure of powder and sintered samples was studied by scanning electron microscopy SEM (XL 30, Philips). Phase composition was measured at room temperature by X-ray diffraction technique using CuK_α radiation (D500 Diffractometer, Siemens) and the amount of phases was calculated from tetragonal and monoclinic (111) peaks in X-ray diffraction spectra using Nickolson-Garvie equation [28].

2.2. Preparation of membranes

Supported membrane consisted of three layers. The support and intermediate layers were alumina and the top and selective layer was zirconia (3Y-ZrO_2). The supported membranes had an asymmetric structure, which is the most frequently used configuration in composite membranes. In asymmetric membrane, the pore size and the thickness of layers decrease from support to the top layer for each successive layer. To reduce the pressure drop across the selective layer it is important to have as thin as possible top layer. Since the thin selective layer is brittle and can not stand the service condition, a thick porous substrate with large pores provides the required strength (the support layer). The pressure drop in the support layer with large pores is low. Particles of the top layer should not get inside the support pores in processing since it drops the permeability of the asymmetric membrane. For this reason intermediate layer is added between the support and top layer.

To prepare zirconia asymmetric membrane, the alumina support was prepared by uniaxial pressing. The support layer had pores of 35 μm in diameter (mean size) and a thickness of 3 mm after sintering at 1350 °C. In the intermediate alumina layer, pore size was centered at 1 μm and the layer thickness was around 200 μm after sintering at 1300°C. The top or selective zirconia layer had the target median pore size of 0.1–0.3 μm and a thickness of around 60–80 μm. The interface between the top layer and the intermediate layer was sharp and had a good adherence.

Slip casting was used to produce supported and unsupported zirconia membranes. Making a well-dispersed and agglomerate free slip is a crucial step in membrane processing. Aqueous colloidal suspension was prepared by adding ammonium polyelectrolyte PMAA (Darvan C) as dispersant and PVA (polyvinyl alcohol) and glycerol were added as binder and placticizer to increase the green strength and to confer the flexibility of green body. Details of the slip processing and preparation of supported membranes are reported elsewhere [29, 30]. The aqueous zirconia slip was applied by spraying technique on the sintered alumina intermediate layer. The sprayed layer was formed on the intermediate layer by consolidation of the particles after removal of water by capillary action of the layer. Important parameters in slip casting process are the pore size of the support, the solid concentration of slip, the rheology of the slip, and the spraying parameters.

Unsupported samples were cast on a porous mold of plaster as slabs of planar shape in a mold with 10 mm height, 20.5 mm width and 75 mm length.

2.3. Sintering experiments

Thermogravimetric analysis was accomplished using 10°C/min heating rate (DTA/TG, Netzsch STA 409). Sintering kinetics was studied by using constant rate heating dilatometry (Adamel DI-24, Adamel Lhomargy) at a heating rate of 10°C/min. The result of this experiment was corrected for the difference in the thermal expansion of alumina holder and push rod with zirconia. Samples were isothermally sintered in air at 1000°C to 1400°C for holding times of up to 10 h. Heating up and cooling down rates in isothermal sintering were 5° C/min.

2.4. Porous structure analysis

The density of unsupported membranes was measured by Archimedes' method using water immersion technique. Mercury porosimetry (Poresizer 9320, Micromeritics) was used to measure the porosity and pore size distributions in unsupported membranes. The pore size distribution in supported membranes was measured by permporometry method, using a wet-dry flow porometer. In this method, pores filled with alcohol are emptied as the incremental air pressure reaches the pressure needed to push the fluid out of pores of certain size ($r_p = 2\sigma \cos\theta / \Delta P$). Pore size reported in this study is pore diameter. Deionized water has been used at room temperature for measuring the permeability of supported membranes. Microstructural development was studies by SEM. Microhardness was measured by Vickers indentation method (Shimadzu microhardness tester, Type-M) with 300 g load and 15 s hold at the maximum load. The reported values are averages of 10 measurements.

3. Results and discussions

3.1. Powder characteristics

Micrograph of the as-received powder shows spherical shape of particles (Fig. 1). Packed agglomerates and clusters of particles can be seen in the micrograph. Finer particles seem to stick to the bigger ones making aggregates of up to 2 μm. The particle size distribution of dispersed powder shows a monomodal distribution centered at 0.79 μm (Fig. 2). In this size distribution, the primary particle size and also a fraction of hard agglomerates that resisted the dispersing treatment are

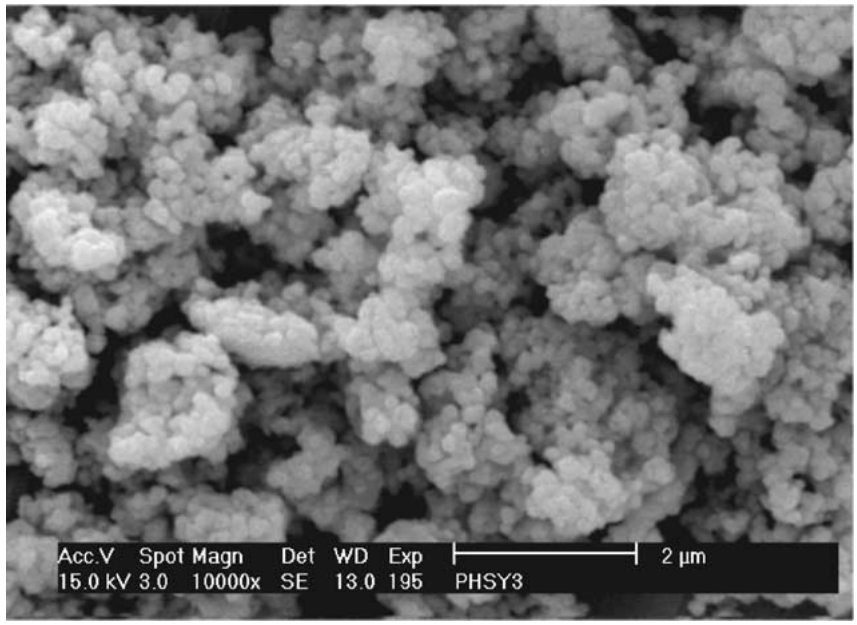

Figure 1 SEM micrograph of HSY3 powder.

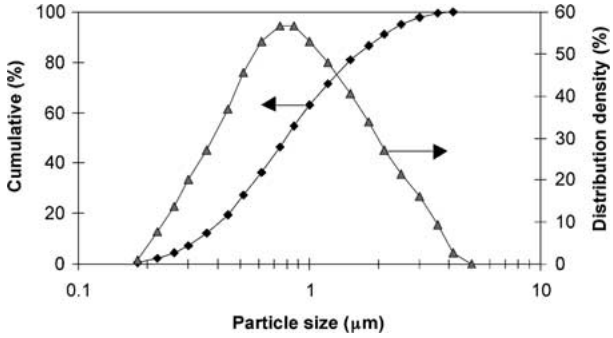

Figure 2 Particle size distribution of HSY3 powder.

present. The ratio of X_{90}/X_{10}, which is an index to evaluate the extent of size distribution, is around 6 in this powder. As shown in Table I, the level of impurities is not high in this powder compared to the other powders of the same composition and the powder has a dual phase structure. The crystallite size of particles is not very fine to suggest grain growth during the early stages of sintering.

TABLE I Some of the most important powder characteristics

HSY3	
Particle size, μm (X_{10}, X_{50}, X_{90})	0.33, 0.79, 2
Specific surface area, m^2/g	6.9
ZrO_2, wt%*	92.6
Y_2O_3	4.5
Al_2O_3	0.3
SiO_2	0.1
Fe_2O_3	0.03
Na_2O	0.03
Cl	0.04
Phase composition (vol.%)	74% t + 26% m♦
Crystallite size[1], nm	100

*The balance in chemical composition is mainly hafnia and some minor impurities.
♦t and m refer to tetragonal and monoclinic phases.
[1]Data from supplier.

3.2. Constant-rate heating (non-isothermal)

Thermogravimetry (TG) curve in Fig. 3a shows less than 3 wt% total weight loss during heating up to 1200°C which is in agreement with the sum of additives used to prepare this sample. When the sample is heated up water and organic components are removed in the first step. About 2% mass reduction was due to the removal of organic components between 220°C and 500°C. The ammonium base polyelectrolyte (PMAA) that was used as dispersant burns out completely up to 550°C in air atmosphere [31]. The heating rate used in this experiment (10°C/min) was too fast for the binder burnout step and it is possible that part of PVA has

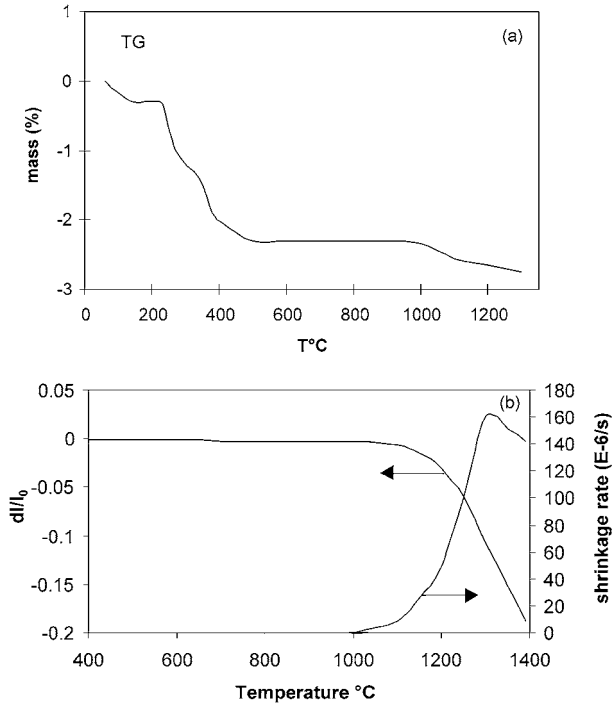

Figure 3 Thermogravimetry (a) and dilatometry results (b) of 3Y-ZrO_2 green membrane during sintering in air atmosphere.

burned at higher temperatures. The small weight loss at about 1000°C, can be partly attributed to the loss of residual chlorine that often exists in the zirconia powders made by the chlorine process [32]. Also part of weight loss at this temperature is possibly from the residual carbon in the form of carbonate or oxycarbonate groups remained from binder burnout that burns at temperatures above 900°C [33].

The continuous shrinkage record of unsupported membrane as a function of temperature is shown in Fig. 3b. Shrinkage of unsupported membrane started at 1000°C. The densification rate increased at about 1100°C and showed a maximum around 1300°C. The highest shrinkage rate was found between 1200°C and 1300°C. Above 1300°C, the shrinkage rate decreased, that can be attributed to the contribution of a grain growth mechanism. The shrinkage curve was uniform and did not show steps as a function of temperature above 1000°C. The presence of one peak in the shrinkage rate indicated a uniform removal of pores and the development of a monomodal pore size distribution in the sample which was also verified later in measured pore size distribution. Different ranges of pore sizes e.g. in bimodal pore size distribution, results in steps in the shrinkage curve [20]. Shrinkage in porous body first starts in agglomerates since the driving force is higher due to the high pore coordination number inside agglomerates [17, 25]. At higher temperatures, inter agglomerate densification will follow.

Sintering of ceramics can be divided into three stages; initial, intermediate and final stage [34]. In sintering of porous membranes, usually sample is heated up to a temperature in which necks between particles provide sufficient strength to the porous body to withstand certain service conditions, with the minimum of pore growth and removal of porosity. In the initial stage, necks are formed by diffusion between adjacent, touching particles [35–36]. The neck formation increases the mechanical strength of the compact but leads to little actual densification [37]. In this stage of sintering, the shrinkage is usually only few percent and the neck length is less than 20% of the particle radius [38]. Pore smoothening also occurs in the initial and intermediate stage of sintering. The initial stage of sintering is essentially insensitive to pore structure but in the intermediate and final stage the shrinkage is dependent on pore structure [24]. Rhodes [39] suggested that, grain boundary or surface diffusion may dominate the initial stage of sintering of yttria stabilized zirconia.

The initial stage of sintering of 3Y-TZP membrane was evaluated on the basis of the shrinkage in non-isothermal sintering. According to Young and Cutler [40], the initial stage of sintering with constant-rate heating can be described by the expression:

$$\ln[(\Delta l/l_0)/T] = -nQ/\mathrm{R}T + C \qquad (1)$$

where $\Delta l/l_0$ is the fractional shrinkage of the compact at temperature T, Q is the activation energy, C and n are constants related to the powder geometry and the sintering mechanism, respectively. Plotting the experimental data for $\ln(\Delta l/l_0)/T$ vs. $1/T$, the Arrhenius

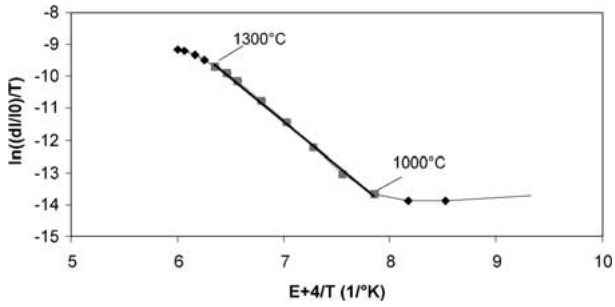

Figure 4 Arrhenius plot for densification in unsupported membrane sintered non-isothermally in dilatometer.

plot, exhibits a single slope line in a range of temperature. The activation energy can be calculated, assuming n according to the dominant mechanism of densification. A change in slope of the curve is caused by a change in mass transport mechanism or by a change in the relative importance of competing mechanisms as well as change in particle size distribution [40]. Stages of sintering can be distinguished from this plot as the slope of the line changes when the particle size distribution is constant. To calculate the activation energy of sintering, in polycrystalline 3Y-ZrO_2, grain boundary diffusion was assumed as the dominant mechanism of material transport at 1000°C to 1300°C, for which n is 1/3. However, in this range of temperature other mechanisms such as surface and volume diffusion are also active. In the formation and growth of neck between particles grain boundary diffusion requires also the cooperation of surface diffusion mechanism.

The data calculated from dilatometry results is presented in Fig. 4. The slope of line changed at 1000°C, below which the surface diffusion mechanism in the initial stage of sintering was dominant. Above 1300°C the change of slope indicated a change in the importance of material transfer mechanisms. The activation energy of sintering calculated for grain boundary diffusion mechanism, between 1000 to 1300°C, was 735 kJ/mol. This value was higher than what other researchers obtained for the densely packed Y-TZP. Using the same equation Wang and Raj [41] found Q equal to 615 ± 80 kJ/mol for 2.8Y-TZP. Young *et al*. [40] assuming the grain boundary diffusion, found an activation energy of about 377 kJ/mol for yttria stabilized zirconia. Sakka [42] measured the activation energy for grain boundary diffusion in $0.16Y_2O_3 - 0.8Zr_{1-x}Hf_xO_2$ at about 309 KJ/mol. Duran *et al*. [43] found an activation energy of 300 kJ/mol for nanocrystalline Y-TZP powders in the intermediate densification step and correlated it with the grain boundary diffusion mechanism. Theunissen *et al*. [44] reported the values of $Q = 275$ kJ/mol for a commercial Y-TZP in the high shrinkage rate range of temperature.

Higher activation energy obtained in 3Y-ZrO_2 membrane, can be explained by the type of pore removal/shrinkage in membrane, the rearrangement of particles and activated sintering due to higher surface area in porous structure. In the membrane, due

to the narrow and monomodal pore size distribution, shrinkage of the pores around the median diameter results in a high shrinkage in small range of temperature, that increases the slope of the line in Arrhenius curve and gives a high activation energy. Particle rearrangement is enhanced in membrane especially around large pores because loosely packed particles are more mobile. The formation and growth of neck between particles occur when there is mass transport from grain boundaries to the neck and then from neck to the free surfaces. Activation energy of sintering is higher for mass transport from the grains in the neck to the free surfaces. The mean diffusion distance is smaller when there are more pores in a body [45]. Therefore shrinkage is enhanced in porous body and yields higher activation energy.

3.3. Microstructure and phase composition

Microstructure of the unsupported membranes sintered at 1100°C to 1400°C is shown in Fig. 5. Neck growth is evident at 1100°C in Fig. 5a. Smoothening of the pore surfaces can be seen in the microstructures above 1100°C. Micrograph of sample sintered at 1200°C shows further growth of neck between particles (Fig. 5b). Higher densification in the agglomerates can be seen in Fig. 5. At 1300°C, pore coordination number; i.e. the number of touching particles surrounding a pore, increased and the pore walls were consisted of many particles (Fig. 5c). Pore growth was noticed at 1300°C and 1400°C. The tortuosity of the membrane decreased as a result of smoother pore surfaces and pore evolution as the sintering temperature increased. Grain growth was evident in the micrographs of samples sintered above 1300°C as suggested by the lower shrinkage rate above 1300°C (Fig. 3b). The grain growth is controlled and hindered by a solute drag mechanism in 3Y-TZP, due to the segregation of yttria in the grain boundaries [46]. Low grain growth indicates that the mobility of pores was higher than that of grain boundaries. Also impurities through their effects on diffusion rate and grain boundary mobility influence the grain growth of Y-TZP [15].

Monoclinic phase that was present in the starting powder transformed to tetragonal phase during heating of the green membrane. XRD spectra of the powder and samples heated at different temperatures are shown in Fig. 6. Monoclinic peaks of (111) at both sides of 30° 2θ, decreased in intensity at 950°C and vanished completely at 975°C. The transformation temperature of monoclinic to tetragonal in heating depends on the amount of yttria as stabilizer, as well as the particle size of powder and occurs in a narrow range of temperature [47]. Supported samples sintered above 975°C after cooling down to room temperature had a 100% tetragonal phase structure. To obtain fully stabilized tetragonal structure at room temperature the grain size must be less than 0.8 μm for 3Y-ZrO_2 [48]. It was reported that some oxide impurities in Y-TZP powder such as sodium, and ferric oxides (present about 0.03 %wt in HSY3 powder) when appeared above 0.01 %wt have some effects on the stability of tetragonal phase during sintering [15].

3.4. Isothermal shrinkage in unsupported membranes

Dimensional shrinkage of the slabs of unsupported membranes is shown in Fig. 7a as a function of sintering temperature and holding time at 1200°C. Sample sintered at 1100°C had a low volume shrinkage (Fig. 7b) that was similar in all dimensions (Fig. 7a). As the sintering temperature increased to 1200°C, shrinkage increased in width and length but not in the thickness of sample sintered for 1 h. Increase of the holding time at 1200°C from 1 h to 3 h resulted in a significant increase in shrinkage in thickness and dimensional shrinkage reached to the same level after 10 h sintering in all directions. Sample sintered at 1300°C showed the highest shrinkage in thickness.

A model for pore evolution in the powder compact was drawn based on the results in shrinkage, as the densification proceeded. In the compact of spherical particles, before the neck formation starts, pores have the shape of the space between the particles with the sharp edges. After the formation of necks, the spheroid pores with smooth corners are formed between the particles. In micro scale differential densification due to the particle size distribution in the powder (finer particles sinter first) and the presence of agglomerates, results in inhomogeneous densification. In macro scale higher shrinkage in lateral dimension at 1200°C/1 h changes the spheroid shape of pores to tubular (elongated), interconnected pores perpendicular to the mold. Tubular pores shrink in the length, when the shrinkage increases in thickness by further increase in sintering temperature or holding time. Winnubst *et al*. [49] also reported that after extensive inter-particle neck formation, an interpenetrating network of tubular pores open to the external surface was developed in the porous sample. Coble [50] stated that in the ideal case, these open tubular pores shrink in radius, though not in length, thereby leading to sample densification. This microstructure is characteristic of the intermediate stage of sintering. Volume shrinkage of unsupported membranes showed a linear increase as a function of sintering temperature and holding time at 1200°C (Fig. 7b).

3.5. Pore size and pore size distributions

Median pore size of the supported membranes increased with increasing the sintering temperature. Unsupported membranes showed no increase in the mean pore size up to 1100°C and further increase in sintering temperature resulted in a decrease in pore size (Fig. 8). A decrease in the mean pore size was expected as a function of sintering temperature above 1000°C where shrinkage started. Pore shrinkage and growth depend on the pore coordination number (R); i.e. the number of particles around a pore [51]. For a given dihedral angle, a critical coordination number R_c exists. Large coordination number ($R > R_c$), is in favor of pore growth e.g. in inter agglomerate pores and small coordination number ($R < R_c$), e.g. in intra agglomerate pores results in pore shrinkage. Pore coordination number is in favor of pore shrinkage in porous body when the condition $R < R_c$ is dominant. In unsupported membrane since

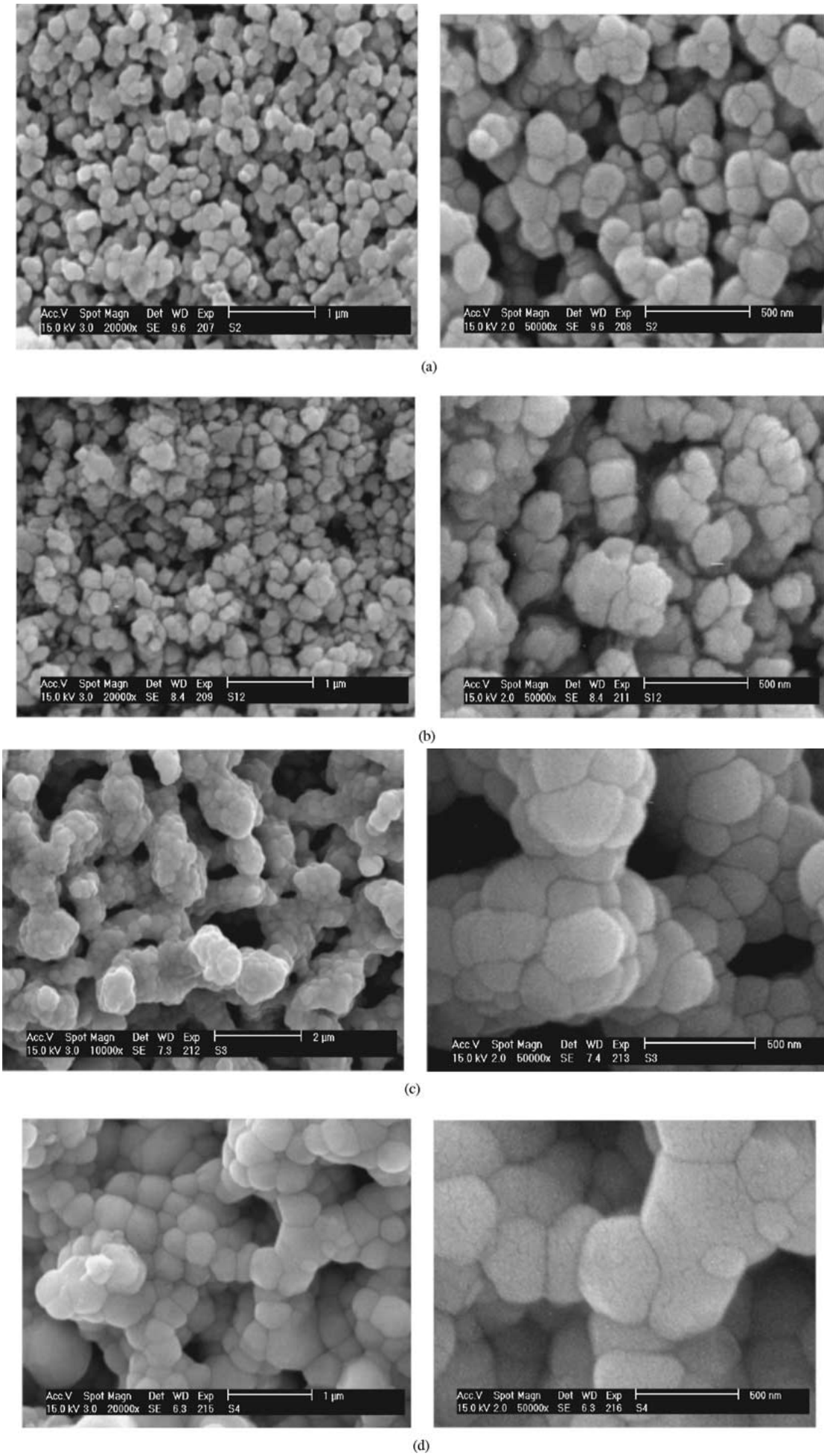

Figure 5 Microstructures of 3Y-TZP membranes sintered at a) 1100°C, b) 1200°C, c) 1300°C and d) 1400°C for 3 h.

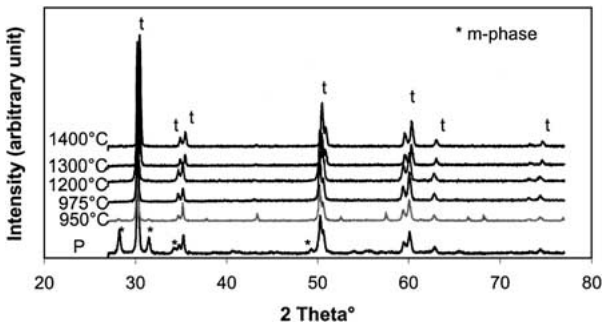

Figure 6 XRD spectra of HSY3 powder (marked by P) and supported membranes sintered at different temperatures for 3 h.

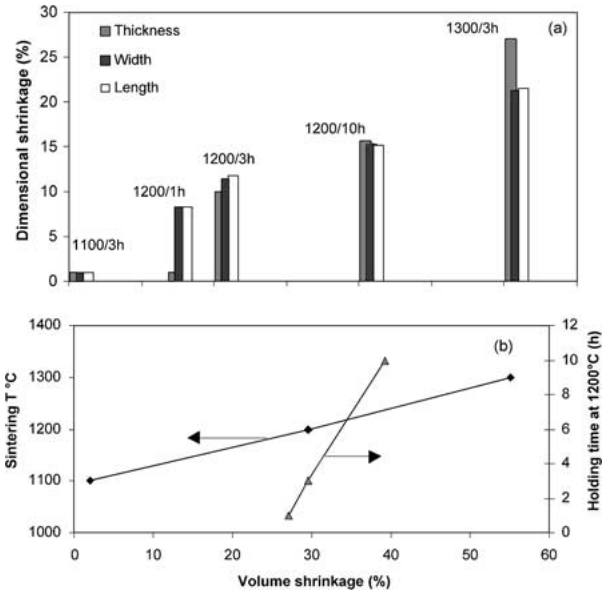

Figure 7 Dimensional shrinkage (a) and volume shrinkage (b) of unsupported membrane slabs sintered at 1100–1300°C for 3 h and at 1200°C for 1, 3 and 10 h.

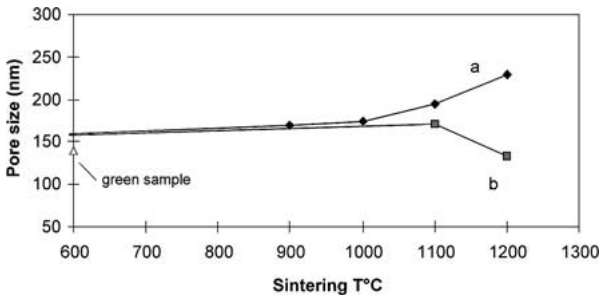

Figure 8 Pore sizes of supported (a) and unsupported (b) membranes as a function of sintering temperature for 3 h holding time. Pore size of the green sample is marked on Y axis.

the coordination number and pore size was not in favor of pore growth, pore size remained stable up to 1100°C and overall shrinkage from 1100°C to 1200°C resulted in lower pore size. Zheng *et al*. [52] introduced a criterion for pore growth based on the ratio of pore size to particle size in green sample that indicated pore growth for the ratios above 0.5. In our case, the ratio of mean pore size to the mean particle size in green sample was 0.2, which should result in pore shrinkage in the early stages of sintering. Pore coordination number and grain size distribution change during sintering

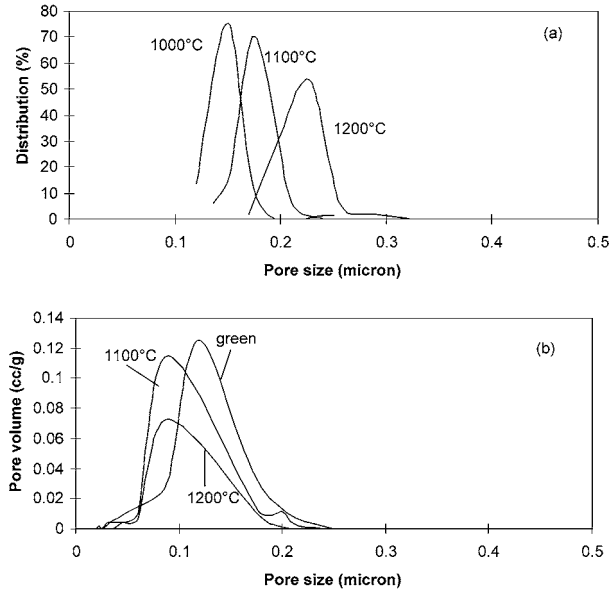

Figure 9 Pore size distribution of supported (a), and unsupported (b) membranes sintered at 1000°C, 1100°C and 1200°C for 3 h.

due to mass transport of material, pore evolution and rearrangement processes [51].

In supported membrane, the shrinkage of top layer during sintering is restricted in lateral dimensions due to the engagement to the rigid support (pre-sintered intermediate layer). As sintering temperature increases, since the support layer restricts the lateral shrinkage, pore growth occurs to accommodate the overall shrinkage in supported membrane (Fig. 8).

Pore size distribution of supported membranes showed a shift to higher pore size as the sintering temperature increased from 1000°C to 1200°C (Fig. 9a). On the other hand, the unsupported membrane showed a shift of pore size distribution to lower pore sizes as the sintering temperature increased up to 1200°C (Fig. 9b). Pore size distribution in both supported and unsupported membranes was monomodal.

3.6. Removal of porosity in isothermal densification

The removal of porosity was low at 1000°C, and increased above 1100°C as a function of sintering temperature or holding time in unsupported samples (Fig. 10a). The change in porosity occurs as a function of sintering temperature and indicates the pore removal and pore coalescence. The effect of holding time to increase the removal of porosity was not pronounced at 1000°C–1100°C that the shrinkage or the shrinkage rate was low. At the temperature that the shrinkage rate was high and above 1150°C, the increase in holding time resulted in higher removal of porosity.

Relative density as a function of holding time showed a linear increase for the holding times up to 10 h (Fig. 10b). The slope of this line increased as the sintering temperature increased from 1000°C to 1300°C, indicating higher influence of holding time on densification. The increase in density as a function of holding time was low at the temperatures where shrinkage was low.

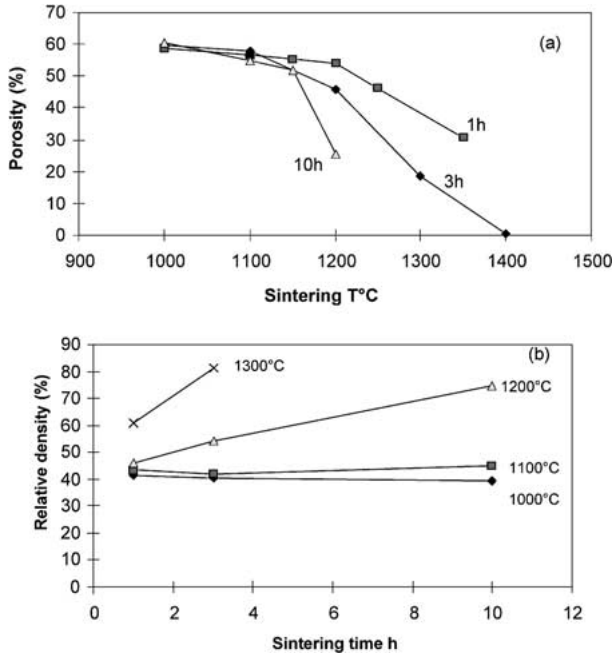

Figure 10 Effect of sintering temperature on porosity for 1 h, 3 h and 10 h holding time in unsupported membranes (a) and the density of unsupported membranes vs. sintering time at 1000°C–1300°C (b).

Low densification at 1000°C, that exhibited no change as a function of sintering time, suggested the initial stage of sintering, in which sintering is independent of porosity [52]. Above 1100°C, in the intermediate stage of sintering the shrinkage rate is high and is influenced by the agglomerate size. In this range of temperature, porosity and pore structure undergo vital changes.

3.7. Microhardness

Supported and unsupported membranes sintered up to 1100°C, at the temperatures that shrinkage and removal of porosity were low, showed the same microhardness. As the densification enhanced above 1100°C, microhardness of supported and unsupported membranes showed a difference. Increase in hardness of supported membranes as the sintering temperature increased was lower than that of unsupported membranes sintered above 1100°C (Fig. 11). Microhardness is sensitive to the progress of densification. The increase in temperature during sintering decreases the porosity, and increases the hardness and mechanical strength due to the growth of necks between particles and removal of porosity. The increase in microhardness was pronounced at the sintering temperatures above 1100°C in which shrinkage started to rise. Lower hardness of supported membranes is attributed to the restricted shrinkage in lateral dimensions. The increase in hardness of unsupported membranes as a result of an increase in holding time from 3 h to 10 h, was also pronounced above 1100°C.

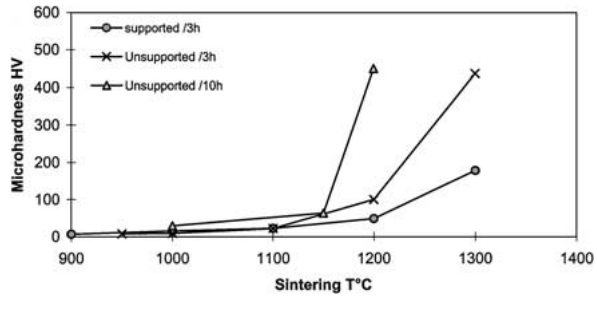

Figure 11 Microhardness (Vickers HV) of supported membranes sintered for 3 h and unsupported membranes sintered for 3 h and 10 h as a function of sintering temperature.

The hardness of unsupported sample sintered at 1200°C for 10 h and that of sample sintered at 1300°C for 3 h, was the same. Although the porosity of sample sintered at 1200°C for 10 h was about 7% less than that of sample sintered at 1300°C for 3 h (Fig. 10a). It indicated the advantage of sintering at lower temperature (above the temperature that removal of porosity starts), for longer period when enhanced hardness is required in order to save some porosity. In the membranes, it is desirable to have required hardness to stand the service conditions and retain as high porosity as possible to increase the permeability.

3.8. Permeability

The permeability of supported membranes as a function of sintering temperature showed an increase (Fig. 12). Typically, the liquid permeability (flux) is obtained with water as permeate and is expressed in terms of l/h.m2.bar. Permeability is a function of pore size and pore size distribution, porosity, tortuosity, the chemical nature of the membrane and the interaction between membrane and the filtered liquid. It is directly correlated to the squared pore size, porosity and differential pressure across the selective layer and is inversely correlated to the viscosity of permeate and the thickness of membrane. Permeability is often described by the Kozeny-Carman model in which pores are assumed to be capillaries with a common equivalent diameter that is obtained from the surface area and total porosity [53].

Tortuosity is defined by pore shape, connectivity and length of pore channels. It is obvious that tortuosity factor is changing as a function of sintering temperature and holding time. Removal of fine pores, smoothening of pore walls and pore growth in the initial and intermediate stages of sintering resulted in a decrease of tortuosity and enhanced the permeability. As the sintering temperature increases in supported membrane, porosity decreases that lowers the permeability but on the other hand, mean pore size increases and tortuosity

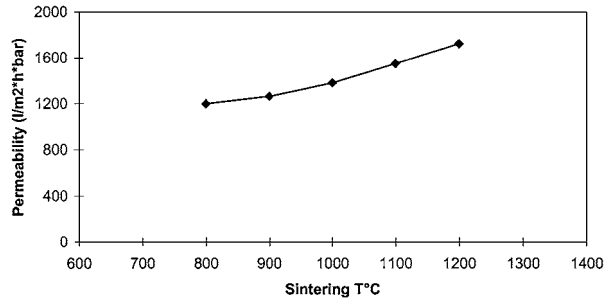

Figure 12 Permeability of supported membrane as a function of sintering temperature (3 h holding time).

decreases, to compensate the effect of porosity and results in an overall increase in permeability as a function of sintering temperature (Fig. 12).

4. Conclusion

In non-isothermal sintering, shrinkage rate increased from 1000°C to 1300°C and showed the highest rate at 1200°C to 1300°C although decreased above 1300°C due to the grain growth. The effect of holding time on the removal of porosity, pore growth and the increase in microhardness was also high in this range of temperature. The activation energy of sintering obtained from non-isothermal shrinkage data was higher than the activation energy reported for dense 3Y-TZP. It was attributed mainly to the removal/shrinkage of large number of pores in a short range of temperature in Y-TZP membrane and the rearrangement of particles during sintering.

Isothermal sintering of unsupported membranes showed that shrinkage and removal of porosity was low in samples sintered at 1100°C and did not change much with the increase in holding time up to 10 h. Different shrinkage was found in lateral and thickness in unsupported membranes as a function of sintering temperature and holding time at 1200°C. Densification increased significantly at 1200°C and higher temperatures and showed higher increase as the holding time increased. Pore shrinkage was found in unsupported membranes sintered at 1200°C, as well as a shift to lower sizes in size distribution.

In supported membranes, pore growth occurred as the densification increased from 1000°C to 1200°C and pore size distribution shifted to higher values. Phase transformation from monoclinic structure to tetragonal structure completed at 975°C and samples sintered at higher temperatures retained a 100% tetragonal structure at room temperature. Hardness of the supported and unsupported membranes was the same up to 1100°C and deviated further as the sintering temperature increased up to 1300°C. Hardness of unsupported membranes sintered above 1100°C was higher. Pore growth and lower hardness in supported membranes were attributed to the restricted shrinkage of supported membranes due to the engagement in the pre-sintered, rigid intermediate layer. Permeability increased in supported membranes as the sintering temperature increased despite the decrease in porosity, due to the pore growth and lower tortuosity.

Acknowledgement

The financial support of The Academy of Finland, through Matra program is greatly acknowledged. Jussi Laurila is acknowledged for performing SEM observations.

References

1. R. BHAVE, "Inorganic Membranes" (Van Nostrand, New York, 1991).
2. A. LARBOT, J.-P. FABRE, C. GUIZARD and L. COT, *J. Amer. Ceram. Soc.* **72** (1989) 257.
3. L. COT, C. GUIZARD and A. LARBOT, *Industrial Ceramics* **8**(3) (1988) 143.
4. C. LIJZENGA, K. KEIZER, M. H. B. J. HUIS VELD, A. J. BURGGRAAF and M. A. ANDERSON, *Key Engineering Materials* **61 & 62** (1991) 383.
5. R. C. GARVIE, *J. Phys. Chem.* **82** (1978) 218.
6. M. HIRANO, *Br. Ceram. Trans. J.* **91** (1992) 139.
7. M. YOSHIMURA, T. HIUGA and S. SOMIYA, *J. Amer. Ceram. Soc.* **69**(7) (1986) 583.
8. T. T. LEPISTÖ and T. A. MÄNTYLÄ, *Ceram. Eng. Proc.* **10**(7–8) (1989) 658.
9. J. F. JUE, J. CHEN and A. V. VIRKAR, *J. Amer. Ceram. Soc.* **74**(8) (1991) 1811.
10. A. J. BURGGRAAF and L. COT, "Membrane Science and Technology Series 4" (Elsevier Science B.V., 1996).
11. R. SINGH, C. GILL, S. LAWSON and G. P. DRANSFIELD, *J. Mater. Sci.* **31** (1996) 6055.
12. M. M. R. BOUTZ, A. J. A. WINNUBST and F. HARTGERS, *ibid.* **29** (1994) 5374.
13. K. HABERKO, *Ceramurgia International* **5**(4) (1979) 148.
14. J. ALLEMAN, H. HOFMANN and L. GAUCKLER, *cfi/Ber. DKG* **67**(1) (1990) 434.
15. J. L. SHI, T. S. YEN and H. SCHUBERT, *J. Mater. Sci.* **32** (1997) 1341.
16. D. H. KIM and C. H. KIM, *J. Amer. Ceram. Soc.* **75**(3) (1992) 716.
17. J. XING-XIANG, H. DONG-SHEN and W. LUQIAN, *J. Mater. Sci.* **29** (1994) 121.
18. D. H. KIM and C. H. KIM, *J. Amer. Ceram. Soc.* **76**(7) (1993) 1877.
19. J. R. SEIDENSTICKER and M. J. MAYO, *J. Amer. Ceram. Soc.* **79**(2) (1996) 401.
20. P. DURAN, M. VILLEGAS, F. CAPEL, P. RECIO and C. MOURE, *J. Eur. Ceram. Soc.* **16** (1996) 945.
21. C. GUIZARD, F. GARCIA, A. LARBOT and L. COT, in Proceeding of the First International Conference on Inorganic Membranes Jul. 89, ICIM '89 Montpelier France, edited by L. Cot and J. Charpin (REGION Languedoc Roussillon) p. 405.
22. A. LARBOT, J. P. FABRE, C. GUIZARD and L. COT, *J. Amer. Ceram. Soc.* **72**(2) (1989) 257.
23. J. RANDON, A. LARBOT, A. JULBE, C. GUIZARD and L. COT, *Key Engineering Materials* **61 & 62** (1991) 495.
24. T. J. CARBONE and J. S. REED, *Ceramic Bulletin* **57**(8) (1978) 748.
25. A. ROOSEN and H. HAUSNER, *cfi/Ber. DKG* **4/5** (1985) 184.
26. V. A. DUBOK, M. I. KABANOVA and N. P. PAVLENKO, *Soviet Powder Metallurgy and Metal Ceramics* **27** (1988) 936.
27. L. GAO, H. C. QIAO, H. B. QIU and D. S. YAN, *J. Eur. Ceram. Soc.* **16** (1996) 437.
28. R. C. GARVIE and P. S. NICKOLSON, *J. Amer. Ceram. Soc.* **55** (1972) 303.
29. F. SHOJAI and T. A. MÄNTYLÄ, in Proceeding of Euromembrane '95, Sep. 1995, UK, p. I-390.
30. *Idem.*, in Proceeding of Forth Euro Ceramics, edited by C. Galassi (Gruppo editoriale Faenza Editrice) Vol. 2, p. 47.
31. T. A. RING, "Fundamentals of Ceramic Powder Processing and Synthesis" (Academic Press, Inc. 1996).
32. C. E. SCOTT and J. S. REED, *Am. Ceram. Soc. Bull.* **58**(6) (1979) 587.
33. M. TAHA, J. PALETTO, Y. JORAND, G. FANTOZZI, A. SAMDI, M. JEBOROUNI and B. DURAND, *J. Eur. Ceram. Soc.* **15** (1995) 759.
34. C. H. HSUEH, A. G. EVANS and R. L. COBLE, *Acta Metall.* **30** (1982) 1269.
35. R. L. COBLE, *J. Amer. Ceram. Soc.* **56** (1973) 461.
36. R. M. CANNON and W. C. CARTER, *ibid.* **72** (1990) 2345.
37. M. J. MAYO, *International Materials Review* **41** (1996) 85.
38. H. E. EXNER and E. ARZT, "Physical Metallurgy" (Elsevier Science Publications BV, Amsterdam, 1983), p. 1885.
39. W. H. RHODES, *J. Amer. Ceram. Soc.* **64** (1981) 19.
40. W. S. YOUNG and I. B. CUTLER, *ibid.* **53** (1970) 659.
41. J. WANG and R. RAJ, *ibid.* **74**(8) (1991) 1959.
42. Y. SAKKA, Y. IOSHI and K. ANDO, *J. Mater. Sci.* **17** (1982) 3101.

43. P. DURAN, M. VILLEGAS, F. CAPEL, P. RECIO and C. MOUR, *J. Eur. Ceram. Soc*. **16** (1996) 945.
44. G. S. A. M. THEUNISSEN, A. J. A. WINNUBST and A. J. BURGGRAAF, *ibid*. **11** (1993) 315.
45. W. D. KINGERY and B. FRANCOIS, in "Sintering and Related Phenomena," edited by G. C. Kuczynski, N. Hooten and C. Gibson (Gordon & Breach Science Publishers, New York, 1967) p. 471.
46. A. J. A. WINNUBST, G. S. A. M. THEUNISSEN, W. F. M. ZEVERT GROOT and A. J.BURGGRRAAF, *Science of Ceramics* **14** (1987) 309.
47. R. RUH, K. S. MAZDIYASINI, P. G. VALENTINE and H. O. BIELESTIN, *J. Amer. Ceram. Soc*. **67** (1984) C-190.
48. F. F. LANGE, *J. Mater. Sci*. **17** (1982) 240.
49. A. J. A. WINNUBST, G. S. A. M. THEUNISSEN, M. M. R. BOUTZ and A. J.BURGGRAAF, in "Structural Ceramics: Processing, Microstructure and Properties" edited by J. J. Bevtzen *et al*. (Roskilde, Riso National Laboratory, 1990).
50. R. L. COBLE, *J. Appl. Phys*. **32** (1961) 787.
51. F. F. LANGE, *J. Amer. Ceram. Soc*. **67** (1984) 83.
52. J. ZHENG and S. REED, *J. Am. Ceram. Soc*. **72** (1989) 810.
53. P. C. CARMAN, *Trans. Inst. Chem. Eng*. **15** (1937) 168.

Received 30 May
and accepted 27 October 2000